Gain Modeling of Strained InGaAsP Based MQW Optical Amplifiers

Grégoire Debaisieux, Moustapha Guemmouri, Sandrine Chelles, Abdallah Ougazzaden, Guillaume Hervé-Gruyer, Marcel Filoche, Jean-Yves Marzin

Gain Modeling of Strained InGaAsP Based MQW Optical Amplifiers

Grégoire Debaisieux, Moustapha Guemmouri, Sandrine Chelles, Abdallah Ougazzaden, Guillaume Hervé-Gruyer, Marcel Filoche, and Jean-Yves Marzin

***Abstract*— Experimental gain spectra of two strained multiquantum-well (MQW) optical amplifiers are compared to theoretical results obtained from Fermi's golden rule and a four-band $k \cdot p$ method. Good agreement is found for both TE and TM modes on each structure.**

***Index Terms*— Integrated optoelectronics, quantum-well devices, semiconductor device modeling, semiconductor optical amplifiers, strain.**

I. Introduction

STRAINED multiquantum-well (MQW) optical amplifiers are now used to implement complex optoelectronic functions, such as wavelength conversion. In those applications, it is important to design polarization independent optical amplifiers and thus to have a reliable gain model that can be used as a design tool.

Theoretical gain calculations in MQW laser or amplifiers have been subject to extensive work [1]–[3]. Theoretical gain is usually derived from Fermi's golden rule, including a Lorentzian line-shape function. In those calculations, valence band mixing is taken into account through the $k \cdot p$ method using a Luttinger–Kohn Hamiltonian. Another problem is the inclusion in the model of many-body effects or bandgap renormalization [4]. However, in those papers, various models are seldom compared to experimental results.

In this letter, good agreement between calculations and experimental gain spectra measured on strained GaInAsP based MQW optical amplifiers is obtained. The theoretical model includes bandgap renormalization. Good agreement between experiment and theory is found for both TE and TM modes.

II. Model

In our model, valence band mixing is taken into account by a 4×4 Luttinger–Kohn Hamiltonian in which strain is introduced through the theory of Pikus–Bir [1]. The effective mass equation is solved with a finite element method. Material gain is calculated by assuming the classical expression derived from Fermi's golden rule and introducing a Lorentzian line-shape function [5] with:

$$G = \frac{e^2\hbar}{\overline{n}\epsilon_0 c m_0^2}\,\frac{1}{\hbar\omega}\,\frac{1}{L_z}\sum_{m,l}\int |M^{m,l}|^2 \cdot \frac{(f_c - f_v)(\hbar/\tau_{in})}{(E_c^m - E_v^l - \hbar\omega)^2 + (\hbar/\tau_{in})^2}\,\frac{k}{\pi}\,dk \qquad (1)$$

where e is the electron charge, $\hbar$ is Planck's constant divided by 2π, $\overline{n}$ is the optical index, ϵ_0 is the vacuum permittivity, c is the free space speed of light, $\hbar\omega$ is the photon energy, L_z is the well width, $|M^{m,l}|^2$ is the optical matrix element [5], f_c (f_v) is Fermi–Dirac occupation probability of electron (hole) in the mth (lth) conduction (valence) subband of energy E_c^m (E_v^l). τ_{in} is the intraband relaxation time. Kane's matrix element is supposed constant and equal to 23 eV.

This model is applied on a single quantum-well neglecting well to well coupling. Flat bands and equal densities of electrons and holes in the well are also assumed. Bandgap renormalization is introduced after calculation of the discrete states and optical matrix elements, as a rigid shift of the discrete energy levels. Since a short range of carrier densities is used to fit our experiments, bandgap renormalization (see δE_g in Tables I and II) is taken independent of carrier density.

Characteristics of the MQW stack were first determined using the photoluminescence (PL) wavelength and the X-ray diffraction spectrum of the active zone. In this procedure PL wavelength is assumed to give the energy transition of the fundamental level. The X-ray diffraction spectrum is treated within the kinematic approximation. This first step of

TABLE I
Fitted Parameters Values for Structure A

Well material	$In_{0.5}Ga_{0.5}As_{0.95}P_{0.05}$
Barrier material	$In_{0.948}Ga_{0.052}As_{0.258}P_{0.742}$
τ_{in} (ps)	0.0375
δE_g (meV)	46.5
Carrier density range ($\times 10^{18}$ cm^{-3})	2.12–2.24

TABLE II
Fitted Parameters Values for Structure B

Parameter	Compressive well	Tensile well
τ_{in} (ps)	0.044	0.0408
δE_g (meV)	18.5	37.5
Carrier density range ($\times 10^{18}$ cm^{-3})	2.0–2.14	2.19–2.33

Manuscript received May 12, 1997; revised July 1, 1997.

G. Debaisieux, M. Guemmouri, S. Chelles, A. Ougazzaden, and G. Hervé-Gruyer are with the France Telecom CNET Laboratory, 92225 Bagneux Cedex, France.

M. Filoche is with the Ecole Polytechnique LPMC Laboratory, 91128 Palaiseau Cedex, France.

J.-Y. Marzin is with the CNRS L2M Laboratory, 92220 Bagneux, France.

Publisher Item Identifier S 1041-1135(97)07930-5.

device characterization gave us well and barrier widths and an allowed range for material compositions.

Since too few data can be found in the literature for strained GaInAsP MQW structures, we also considered as fit parameter the intra-band relaxation time τ_{in} that determines the width of the Lorentzian line-shape function. Furthermore, since we had no reliable relationship between current in the device and corresponding average carrier density in the active zone, carrier density was also included in our fit parameters. A summary of all fit parameters can be found in Table I.

Device theoretical modal gain spectrum is derived from theoretical material gain spectrum from the length of the device, an estimation of the intrinsic losses and optical confinement factors for TE and TM modes estimated with a one-dimensional (1-D) model. In this derivation, longitudinal effects are neglected.

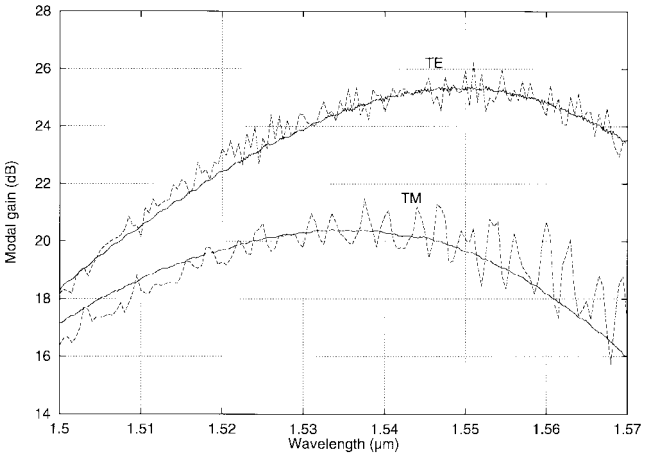

Fig. 1. Measured TE and TM ASE spectra (solid) compared to measured TE and TM fiber to fiber gain spectra (dashed) for structure B at 60 mA.

III. Results and Discussion

The model is applied on two different optical amplifiers A and B. Both have a 1.5-μm-wide and about 1-mm-long buried ridge structure. Their growth was performed with atmospheric pressure MOVPE. The active region is embedded between GaInAsP confinement layers and surrounded by thick n-doped and p-doped InP layers to form the p-i-n diode.

In structure A, the active region consists of 18 periods of tensile strained InGaAsP wells and compressive strained InGaAsP barriers. The active region includes two tapers at both device ends and has tilted facets. Device geometry is the same as device geometry presented in [6]. Since the length of the two tapers is less than 10% of the total device length their effect was neglected in our computation. PL wavelength at room temperature is 1.487 μm. Assuming this value corresponds to the transition of the fundamental level E1-LH1, the characteristics of the MQW stack obtained from the X-ray diffraction spectra are 125-Å-thick $In_{0.51}Ga_{0.49}As_{0.92}P_{0.08}$ wells and 60-Å-thick $In_{0.96}Ga_{0.04}As_{0.26}P_{0.74}$ barriers.

Structure B has the same geometry as structure A but has a different active region. The active region consists of four compressive strained quantum wells and three tensile strained quantum wells. If all wells are numbered in ascending order compressive wells are number 1, 3, 5, 7 and tensile wells are number 2, 4, 6. Material of the tensile well is 160-Å-thick $In_{0.4}Ga_{0.6}As$. Material of the compressive well is 100-Å-thick $In_{0.84}Ga_{0.16}As_{0.734}P_{0.266}$. Barrier material separating two wells is 130-Å-thick $In_{0.805}Ga_{0.195}As_{0.392}P_{0.608}$. In this structure, the major contribution of TE gain is due to the compressive strained well, whereas the major contribution of TM gain is due to the tensile strained well. Experimental modal gain is compared to the sum of theoretical modal gain obtained for each type of well.

Intrinsic losses are supposed to be 20 dB·cm^{-1} for both structures. Optical confinement factor are $\Gamma_{TE} = 39.1\%$, $\Gamma_{TM} = 38.5\%$ for structure A and $\Gamma_{TE} = 15.5\%$, $\Gamma_{TM} = 14.6\%$ for structure B.

Experimental gain spectra were obtained by two ways. The first way is by measurement of amplified spontaneous emission (ASE) for different driving currents below the saturation current for both TE and TM modes. This method is relatively easy and a reliable control of the polarization is obtained. The drawback of this method is that only a relative value of modal gain is obtained so that a fitting additive constant to match the calculated modal gain has to be chosen.

The second way is by direct gain measurement, light being injected in the device and collected out by monomode optical fibers. Device gain is then estimated by adding fiber coupling losses to the measured gain. ASE spectra and gain spectra are similar around peak gain for both TE and TM modes for the injection levels used in this paper (e.g., 60 mA, see Fig. 1). This allows us to scale our ASE spectra. Since TE and TM ASE spectra are more easily obtained and present no ripple, we use them to fit theoretical curves.

Since results of gain calculation depend heavily on each of the fit parameters, an important part of the work was dedicated to design a manual fit procedure. Simplification was achieved noticing that: bandgap renormalization mainly governs wavelength at maximum gain for TE and TM modes, material strain mainly governs space between TE and TM wavelengths at maximum gain, τ_{in} parameter and carrier density mainly govern bandwidth and maximum gain value.

Therefore, the first step of our fitting procedure was to adjust simultaneously bandgap renormalization and well and barrier compositions, in order to find the best agreement for wavelength at maximum gain for TE and TM modes. At this step, well and barrier compositions were supposed to be known. Then, τ_{in} parameter and carrier density were adjusted to match both TE and TM maximum gain values and bandwidths, in which step bandgap renormalization was eventually readjusted.

More precisely for structure B, material compositions obtained by X-ray diffraction spectra were not varied. Only carrier densities, bandgap renormalization and τ_{in} parameter in each type of well were adjusted. Since two wells are concerned the fit procedure was much lightened by this restriction.

We finally obtain all fit parameters presented in Table I for structure A and in Table II for structure B. All fitted parameters are acceptable values.

Experimental results and fitted theoretical results are presented for structure A in Fig. 2(a) for TE mode and in Fig. 2(b)

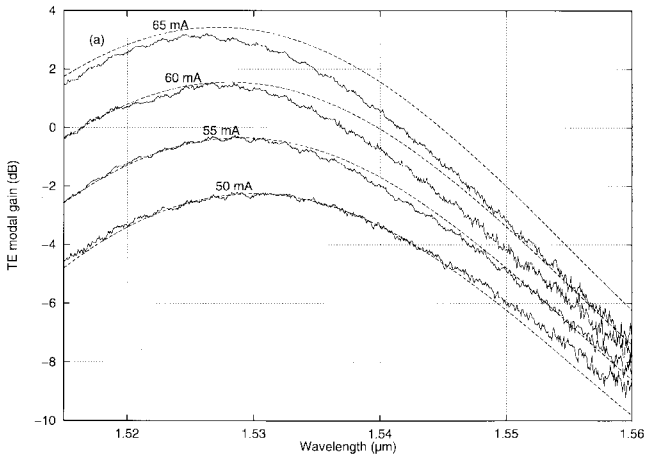

(a)

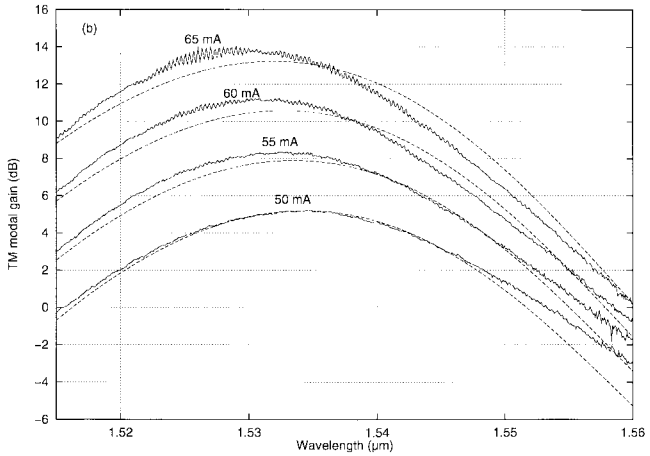

(b)

Fig. 2. Experimental (solid) and theoretical (dashed) (a) TE and (b) TM modal gain spectra for structure A. Carrier densities corresponding to 50-, 55-, 60-, 65-mA injection currents are respectively 2.12, 2.15, 2.18, 2.21 cm $\times$ 10^{18} cm^{-3}.

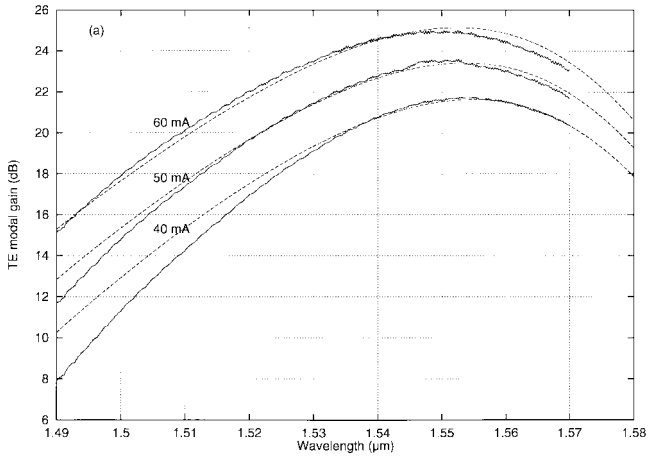

(a)

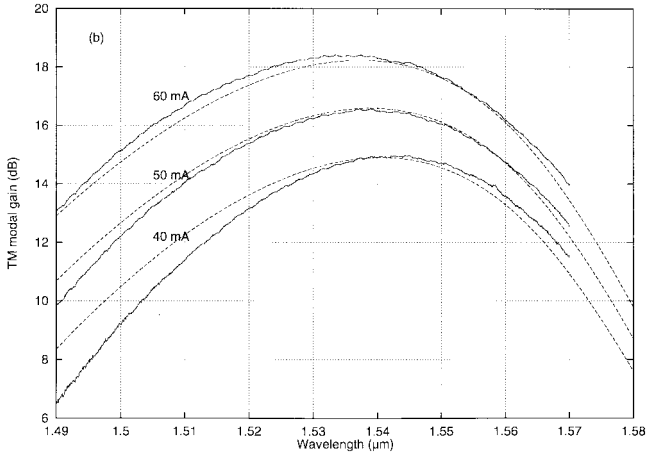

(b)

Fig. 3. Experimental (solid) and theoretical (dashed) (a) TE and (b) TM modal gain spectra for structure B. Carrier densities corresponding to 40-, 50-, 60- mA injection currents are respectively 2.0, 2.07, 2.14 $\times$ 10^{18} cm^{-3} in the compressive well and 2.19, 2.26, 2.33 $\times$ 10^{18} cm^{-3} in the tensile well.

for TM mode. Analog results are presented for structure B in Fig. 3(a) and (b). Good agreement is found on the two structures for both TE and TM modes and for different injection values with the same set of parameters. Experimental curves are presented for various injection currents, below gain saturation, whereas theoretical curves are presented for the matching carrier densities.

IV. Conclusion

Theoretical gain including bandgap renormalization is compared to experimental gain. Band mixing is included using a 4 $\times$ 4 Luttinger–Kohn Hamiltonian and gain is obtained using a Lorentzian broadening model. On each of the two structures analyzed in this letter, good agreement is found for both TE and TM modes with the same set of parameters. Three types of quantum wells are studied in this work, but this amount of data is not enough to draw reliable conclusion on the dependencies of the fit parameters on material composition or strain. Thus, to achieve a predictive ability of the model, future work will investigate results obtained for other MQW optical amplifiers. It is hoped that this model can be used as a CAD tool to design polarization independent MQW optical amplifiers.

Acknowledgment

The authors would like to thank D. Sigogne, S. Slempkes, M. Carré, J. Landreau, and M. Foucher for device fabrication.

References

[1] S. L. Chuang, "Efficient band-structure calculations of strained quantum wells," *Phys. Rev. B*, vol. 43, no. 12, pp. 9649–9661, 1991.

[2] D. Ahn and T.-K. Yoo, "Envelope function calculations of linear and nonlinear optical gains in a strained-layer quantum-well laser," *IEEE J. Quantum Electron.*, vol. 29, pp. 2864–2872, Dec. 1993.

[3] C.-S. Chang and S. L. Chuang, "Modeling of strained quantum-well lasers with spin-orbit coupling," *IEEE J. Select. Topics Quantum Electron.*, vol. 1, pp. 218–229, June 1995.

[4] D. Ahn and S. L. Chuang, "The theory of strained-layer quantum-well lasers with bandgap renormalization," *IEEE J. Quantum Electron.*, vol. 30, pp. 350–365, Feb. 1994.

[5] S. W. Corzine, R.-H. Yan, L. A. Coldren, "Optical gain in III–V bulk and quantum well semiconductors" in *Quantum Well Lasers*, P. S. Zory, Jr., Ed. San Diego, CA: Academic, 1993, ch. 1.

[6] D. Sigogne, A. Ougazzaden, D. Meichenin, B. Mersali, A. Carenco, J. C. Simon, I. Valiente, C. Vassallo, and L. Billes, "1.55 μm polarization insensitive InGaAsP strained MQW optical amplifier integrated with short spot-size converters," *Electron. Lett.*, vol. 32, no. 15, pp. 1403–1405, 1996.